Absolute calibration of the antiproton detection efficiency for BESS below 1 GeV

Y. Asaoka [a,1], K. Yoshimura [b], T. Yoshida [b], K. Abe [a], K. Anraku [a], M. Fujikawa [a], H. Fuke [a], S. Haino [a], K. Izumi [a], T. Maeno [c], Y. Makida [b], N. Matsui [a], H. Matsumoto [a], H. Matsunaga [a,2], M. Motoki [a,3], M. Nozaki [c], S. Orito [a], T. Sanuki [a], M. Sasaki [c], Y. Shikaze [a], T. Sonoda [a], J. Suzuki [b], K. Tanaka [b], Y. Toki [c] and A. Yamamoto [b]

[a] *Department of Physics and International Center for Elementary Particle Physics, The University of Tokyo, Hongo, Bunkyo, Tokyo, 113–0033 Japan*

[b] *High Energy Accelerator Research Organization (KEK), Oho, Tsukuba, Ibaraki, 305–0801 Japan*

[c] *Department of Physics and Graduate School of Science and Technology, Kobe University, Rokkodai-cho, Nada, Kobe, 657–8501 Japan*

Abstract

An accelerator beam experiment was performed using a low-energy antiproton beam to measure the antiproton detection efficiency of the BESS detector. Measured and calculated efficiencies derived from the BESS Monte Carlo simulation based on GEANT/GHEISHA showed good agreement. With the detailed verification of the BESS simulation, results demonstrate that the relative systematic error of detection efficiency derived from the BESS simulation is within $\pm$ 5%, being previously estimated as $\pm$ 15% which was the dominant uncertainty for measurements of cosmic-ray antiproton flux.

Key words: BESS; systematic error of antiproton flux; antiproton detection efficiency; beam experiment at KEK 12 GeV PS; detector simulation; GEANT/GHEISHA
PACS: 95.55.Vj; 98.70.Sa; 95.85.Ry

---

[1] Correcponding author. E-mail: asaoka@icepp.s.u-tokyo.ac.jp. Tel: +81 3 3815 8384 & Fax: +81 3 3814 8806
[2] present address: University of Tsukuba, Tsukuba, Ibaraki, 305-8571, Japan
[3] present address: Tohoku University, Sendai, Miyagi, 980-8577, Japan

1 Introduction

The BESS spectrometer was designed [1,2] and developed [3–6] as a high-resolution spectrometer with the capability to search for rare cosmic-rays and provide various precision measurements of cosmic-ray primaries.

Since 1993, seven balloon flights have been successfully carried out and more than 10^3 antiprotons ($\bar{p}$'s) have been unambiguously detected. This has allowed measuring the energy spectrum of cosmic $\bar{p}$'s [7–10] exhibiting a characteristic peak around 2 GeV, being expected due to the existence of "secondary" $\bar{p}$'s produced by cosmic-ray interactions with interstellar gas. Since at energies below this peak the secondary $\bar{p}$'s show a sharp decrease due to the kinematics of $\bar{p}$ production, this allows performing a sensitive search for a possible component of low-energy "primary" $\bar{p}$'s which could be produced by novel processes such as annihilation of neutralino dark matter or evaporation of primordial black holes [11].

Investigating the origin of low-energy $\bar{p}$'s requires a reduction in systematic errors of the resultant spectrum, as well as a reduction in statistical errors. The dominant source of systematic error in the low energy region (< 1 GeV) is uncertainty in the $\bar{p}$ interaction losses in the instrument. For the BESS detector, we surmised $\pm$ 15% relative error in detection efficiency which is evaluated using a Monte Carlo simulation (BESS MC) [12] based on the GEANT/GHEISHA code [13,14]. The BESS MC incorporates detailed material and detector descriptions such that realistic detector performance is obtained. The original GHEISHA code was modified so that experimental data of $\bar{p}$-nuclei cross sections [15] are reproduced. Proton-nuclei cross sections below 1 GeV are also modified based on the LaRC model calculation [16]. However, estimating systematic error due to interaction losses is difficult because of uncertainties in secondary multiplicity, angular distribution, and detector response; thus making these losses the dominant source of systematic errors of $\bar{p}$ flux, especially in the low energy range. Accordingly, detection efficiency must be directly measured and precisely verified to reduce systematic error in the low-energy region $\bar{p}$ flux.

Considering this, we performed an accelerator beam experiment at the KEK-PS K2 beam line, i.e., the BESS detector was evaluated using a low-energy $\bar{p}$ and proton beam. The main objectives of the beam experiment were as follows:

(1) directly measure detection efficiencies for $\bar{p}$'s and protons;
(2) evaluate the BESS MC simulation;
(3) reduce systematic error in detection efficiency for $\bar{p}$'s.

Simultaneously measuring detection efficiencies for $\bar{p}$'s and protons helps to achieve (2) and (3) because they behave similarly in the instrument except for deflection in the magnetic field and inelastic interactions.

Section 2 briefly summarizes the BESS detector, while Section 3 defines the detection efficiency. Main features of the accelerator beam setup and a summary of collected data are presented next in Section 4, after which Section 5 describes incident beam identification which determines the number of detector incidence particles. Measurement of the detection efficiency is then presented in Section 6, with a comparison between beam data and simulation results being discussed in Section 7 along with an evaluation of systematic error in detection efficiency. Finally, Section 8 summarizes the main results and provides conclusions.

2 BESS Spectrometer

Figure 1 shows a schematic view of the BESS detector. A uniform magnetic

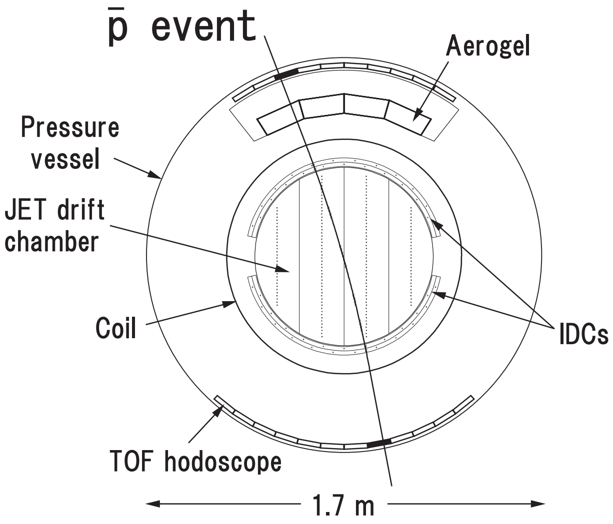

Fig. 1. Cross-sectional view of the BESS detector showing a $\bar{p}$ event.

field of 1 Tesla is produced by a thin (4 g/cm^2) superconducting coil [4], with substantial incident particles passing through without interaction. The magnetic-field region is filled with a tracking detectors composed of a jet type drift chamber (JET) and inner drift chambers (IDCs). This geometry results in an acceptance of 0.3 m^{2}sr, being an order of magnitude larger than those of previous cosmic-ray spectrometers. Tracking is performed by fitting up to 28 hit-points in the drift chambers, resulting in magnetic-rigidity ($R \equiv Pc/Ze$) resolution of 0.5% at 1 GV. Energy deposit in the drift chamber gas is also obtained as a truncated mean of the integrated charges of hit pulses. The upper and lower scintillator-hodoscopes (TOF) [6] provide two dE/dx measurements and the time-of-flight of particles. The instrument also incorporates a threshold-type Cherenkov counter [5] with a silica-aerogel radiator that can identify $\bar{p}$'s from a e^-/μ^- background up to a kinetic energy of 4 GeV. Here, cylindrical coordinates (r, ϕ, and z) and Cartesian coordinates (x, y, and z) are used for representing the BESS instrument, where y and z are respectively the vertical axis and axis of the solenoid.

Although the BESS detector has been successively upgraded since the first successful flight in 1993, the basic concept of particle identification is the same, i.e., mass determination using the rigidity and velocity of incident particles. Accordingly, the presented beam results can be applied to both past and future detectors.

3 Detection Efficiency

The detection efficiency (ε) of $\bar{p}$'s (protons) is defined as

$$\varepsilon = \frac{\mathrm{N_{obs}}}{\mathrm{N_{inc}}},$$

where $\mathrm{N_{inc}}$ is the number of incident $\bar{p}$'s (protons) within the acceptance of the detector, and $\mathrm{N_{obs}}$ is the number of particles identified as $\bar{p}$'s (protons).

Due to the symmetrical detector configuration of the BESS instrument, since non-interacting antiprotons behave like protons except for deflection, we applied the same selection criteria as protons for $\bar{p}$ identification. In flight data, protons are obtained with sufficient statistics using unbiased samples, since they are the most abundant species in cosmic radiation.

Antiproton selection is performed using the following cuts [10]:

(1) select events with a single downward-traveling particle fully contained in the fiducial region of the tracking detectors;
(2) require only one (one or two) hit in the upper (lower) TOF hodoscopes;
(3) require TOF hit position consistency with the $r-\phi$ and y-z trajectory;
(4) require loose $\mathrm{d}E/\mathrm{d}x$ consistency with protons in upper and lower TOF hodoscopes;
(5) require track quality to ensure correct measurements such as reduced chi-square of track fitting;
(6) perform particle identification using reconstructed mass and three $\mathrm{d}E/\mathrm{d}x$ measurements.

$\mathrm{N_{obs}}$ is obtained by applying cuts (1)–(6) to $\mathrm{N_{inc}}$, i.e., together they define detection efficiency. In the analysis of flight data, interaction losses are estimated using the BESS MC, while other efficiencies can be precisely estimated by proton samples. Cuts (1)–(4) are expected to be sufficient to reject all inelastically interacted events which are "visible" in the instrument. If, for example, an interaction occurs at the bottom of the instrument, then it may not be detected by applying cuts (1)–(6) and therefore be "invisible" to the instrument. Together cuts (1)–(4) are denoted as CUT.

The detection efficiency can be decomposed into two factors, i.e.,

$$\varepsilon = \varepsilon_{\mathrm{non-int}} \cdot \varepsilon_{\mathrm{ID}},$$

where $\varepsilon_{\mathrm{non-int}}$ is the efficiency of CUT, called the non-interacting efficiency, and $\varepsilon_{\mathrm{ID}}$ is the efficiency of (5) and (6) after applying CUT, called the identification efficiency. Since no difference exists in $\varepsilon_{\mathrm{ID}}$ between protons and $\bar{p}$'s, the detection efficiency can be expressed as

$$\varepsilon(\bar{p}) = \varepsilon_{\mathrm{non-int}}(\bar{p}) \cdot \varepsilon_{\mathrm{ID}}(\bar{p}) = \varepsilon_{\mathrm{non-int}}(\bar{p}) \cdot \varepsilon_{\mathrm{ID}}(p).$$

Considering the above equations, since $\varepsilon_{\mathrm{ID}}(p)$ can be precisely estimated using flight data, systematic error in detection efficiency can be evaluated using only $\varepsilon_{\mathrm{non-int}}(\bar{p})$ in the beam experiment, although $\varepsilon_{\mathrm{ID}}(\bar{p}) = \varepsilon_{\mathrm{ID}}(p)$ should be confirmed.

4 Experimental

4.1 Beam line setup

The BESS beam experiment was performed in February 1999 at the KEK-PS K2 beam line which is equipped with an electro-static separator [17] to enrich low energy $\bar{p}$'s. The BESS detector was located 8 m downstream of the focal point because the E373 experiment [18] was being run in parallel. The resultant beam profile at the detector was about 20 cm (W) $\times$ 10 cm (H), being a beam spread in which detector performance is uniform. Figure 2 shows a schematic view of the experimental setup. D1 and D2 are dipole magnets and Q1–Q7 are quadrapole magnets used for beam transport and focusing. KURAMA is another dipole magnet for analyzing momentum of incident particles. By adjusting magnet current, the deflection angle at KURAMA was maintained at 8° irrespective of beam momentum. The BESS detector was rotated circumferentially 70° in r-ϕ plane such that it was suitably positioned in the beam line for proper beam incidence.

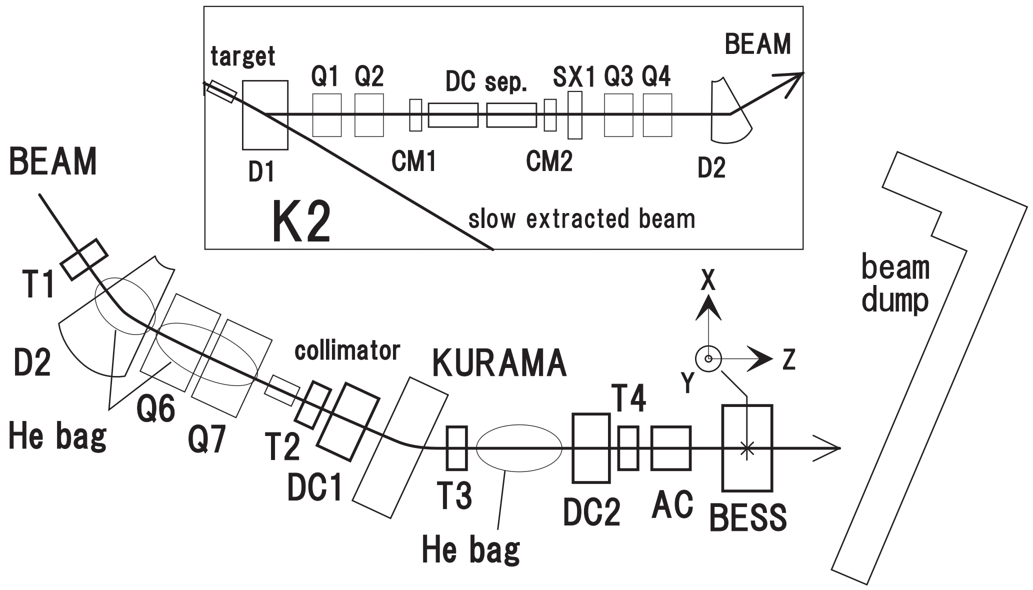

Fig. 2. Experimental setup of K2 beam area for BESS beam experiment.

Other than our detectors, there was more than 3 g/cm^2 of materials in the K2 beam line, thus interaction and energy losses of incident particles cannot be neglected. To reject interacted events and identify incident particles, we placed four trigger counters (T1–T4), two drift chambers (DC1 and DC2), and an aerogel Cherenkov counter (AC) in the beam line. A right-handed coordinate system is obtained in which the z-axis is in the beam direction, the y-axis is vertical and upwards, and the origin is at the center of the BESS detector position. Detector positions are also shown in Fig. 2.

Each trigger counter consists of a 1-cm-thick Bicron BC404 plastic scintillator. Two photomultiplier tubes (PMTs) are mounted on each end of the plastic scintillator through acrylic light guides. Trigger counters are also used for charge-amplitude/timing measurements for off-line analysis. Energy deposit ($\mathrm{d}E/\mathrm{d}x_{\mathrm{T1}}$, etc.) in each counter and particle velocity ($\beta_{\mathrm{T4-T1}}$, etc.) between counters were measured. The timing resolution of each counter is 30 to 40 ps. A wider T4 is used in order to obtain better statistics for low energy $\bar{p}$'s.

Drift chambers (DCs) with a full drift length of 1 cm use a mixture of 50–50 % Ar-ethane gas. Each DC has three planes of wire layers in both the horizontal and vertical plane such that 3D tracking is obtained. The position resolution of each hit is about 150 μm. In order to measure the deflection angle at KURAMA, DC1 and DC2 were placed on both sides of it. The incident position and angle into the BESS detector were obtained from the combined track (referred to as the beam track) fitted DC1 and DC2 hits.

The aerogel Cherenkov counter (AC) uses an 8-cm-thick silica aerogel block with refractive index of 1.03 as a Cherenkov radiator. Light output (Q_{AC}) is collected by four PMTs mounted on the counter. The veto of Q_{AC} is integrated into the trigger system which remarkably improves the $\bar{p}/\pi$ ratio. The AC functions as a threshold type Cherenkov counter during off-line analysis for $\bar{p}/\pi$ separation. The mean number of photoelectrons was about 13, resulting in a rejection factor of more than 10^4. Main parameters of these detectors are summarized in Table 1.

Table 1
Summary of beam line instrumentation.

Detector Name	Fiducial Volume (mm^3)	Location (m)	Resolution
T1	$120_W \times 40_H \times 10^t$	−15.000	30 (ps)
T2	$160_W \times 40_H \times 10^t$	−8.000	30
T3	$180_W \times 40_H \times 10^t$	−5.000	30
NORMAL T4	$180_W \times 40_H \times 10^t$	−2.250	30
WIDE T4	$180_W \times 120_H \times 10^t$	−2.250	40
DC1	$200_W \times 200_H \times 100^t$	−7.853	150 (μm)
DC2	$200_W \times 200_H \times 100^t$	−2.296	150
AC	$300_W \times 190_H \times 80^t$	−1.971	$> 10^4$ (rejection)
BESS	—	0.000	—

Data from the BESS detector and beam line detectors is collected using the BESS data acquisition system. To obtain N_{inc}, instead of using the BESS standard trigger (coincidence between upper and lower TOF counters), the trigger was generated by T1 & T2 & T3 & T4 and $\overline{AC}$. Trigger timing was adjusted such that the difference compared to the BESS standard trigger was less than 5 ns, which did not affect measurable quantities. The trigger rate was kept below several kHz to maintain gain stability of the TOF hodoscopes.

4.2 Beam incidence into BESS detector

Since the BESS detector exhibits uniform performance over a wide region due to the simple cylindrical geometry and uniform magnetic field, there is no need to perform a detailed position/angle scan of detection efficiency. Data was collected for three different detector configurations. The incident beam position was changed by changing BESS configuration in the beam line. Each configuration, i.e., CFG1, CFG2, and CFG3, is shown in Fig. 3. As these configurations were selected to represent the incidence of cosmic-ray particles in terms of the amount of material and penetrated region, a total test of the BESS MC can be performed by combining the data from the three configurations.

The BESS detector cannot be rotated more than 70 ° due to a constraint in the liquid helium storage, and therefore low energy protons ($P_{\rm init} < 1.0 GeV/c$) were out of the BESS acceptance region in this beam experiment.

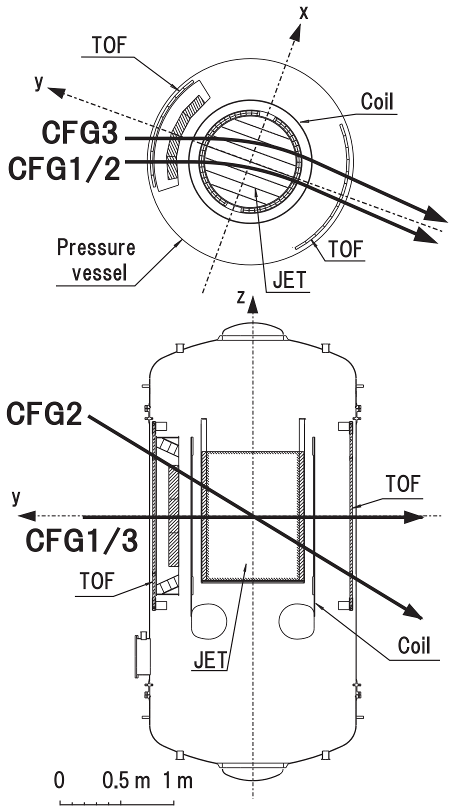

Fig. 3. Cross-sectional view of BESS detector with incident $\bar{p}$ beam for each configuration (CFG1–3). Using CFG1 as a reference, CFG2 is the case in which the incident beam has an angle of $\cos\theta = 0.915$, where θ is defined as the angle between the beam and y-axis in the y-z plane. CFG3 is the case in which the incident beam passes through a different region of the central tracking system in the r-ϕ plane. The distance of incident position between CFG1 and CFG3 is 153 mm along the x-axis.

4.3 Data summary

Table 2 summarizes the collected $\bar{p}$ and proton data. The initial beam momentum ($P_{\rm init}$) is defined by current settings of D1 and D2, which has a momentum spread of ± 3%. Data on pions, deuterons, and helium nuclei were also collected, although data analysis will be reported elsewhere. $\mathrm{CFG1}_{+\mathrm{Al}}$ represents a configuration in which a 30-mm-thick aluminum plate was placed just upstream of the BESS detector. As indicated, initial beam momentum was scanned with each configuration. While more than 10,000 events were collected to obtain sufficient statistics, only about 1,000 events were collected for very low energy $\bar{p}$'s ($P_{\rm init} < 0.70$ GeV/c) due to low production rate and losses during beam transport.

Table 2
Data summary.

BESS Config.	Particle	Initial beam Momentum (GeV/c)	type of T4
CFG1	$\bar{p}$	0.70, 0.80, 1.00, 1.15, 1.30, 1.50, 1.67	NORMAL
CFG1	$\bar{p}$	0.65, 0.66, 0.67, 0.68, 0.69, 0.70	WIDE
CFG1	p	0.70, 0.80, 0.90, 1.00, 1.15, 1.30, 1.50, 1.67	NORMAL
$\mathrm{CFG1}_{+\mathrm{Al}}$	$\bar{p}$	0.80, 1.00, 1.30	NORMAL
$\mathrm{CFG1}_{+\mathrm{Al}}$	p	0.80, 1.00, 1.30	NORMAL
CFG2	$\bar{p}$	0.65, 0.70, 0.80, 1.00, 1.15, 1.30, 1.50, 1.67	NORMAL
CFG2	p	0.70, 0.80, 0.90, 1.00, 1.15, 1.30, 1.50, 1.67	NORMAL
CFG3	$\bar{p}$	0.65, 0.66, 0.67, 0.68, 0.69, 0.70, 0.75, 0.80, 1.00, 1.15, 1.30, 1.50, 1.67	WIDE

5 Analysis

5.1 *Beam identification*

To determine $\mathrm{N}_{\rm inc}$ the beam line detectors must clearly identify the incident particle and precisely determine incident position, angle, and energy. In order to select $\bar{p}$ and proton events, the following cuts were applied on the beam experiment data set:

(1) a good beam track exists in beam line detector DC1 and DC2;
(2) the incident particle has proper deflection angle at KURAMA;
(3) $\mathrm{d}E/\mathrm{d}x$ in T1, T2, T3 and T4 are compatible with $\bar{p}$'s;
(4) $1/\beta$ between T2−T1, T3−T1, T4−T1, T3−T2, T4−T2, and T4−T3 are consistent with that of $\bar{p}$'s;
(5) light particles are rejected by $Q_{\rm AC}$ veto.

Together these cuts are referred to as BID0. The most effective cuts are $1/\beta_{\rm T4-T3}$ and $\mathrm{d}E/\mathrm{d}x_{\rm T4}$ cut, although the $Q_{\rm AC}$ cut is also important because it rejects a part of the interacted events in T4 and AC itself. Figure 4 shows examples for BID0 for $\bar{p}$'s of $P_{\rm init} = 1.67$ GeV/c, where the $1/\beta$ distribution shows a clear separation between $\bar{p}$, kaon, and pion/muon/electron particles which allows incident beam particles to be unambiguously identified.

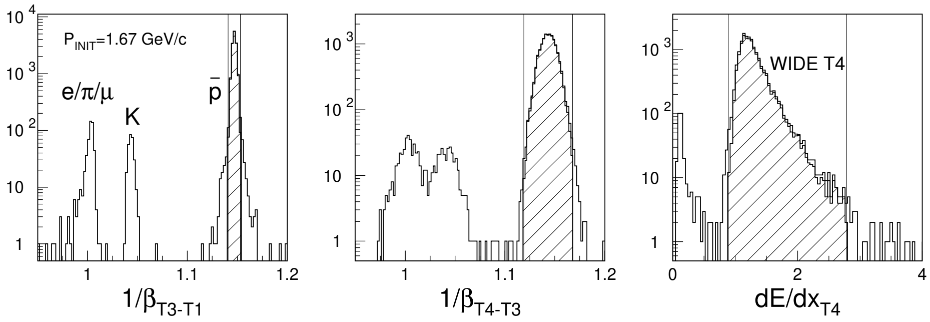

Fig. 4. $1/\beta$ and $\mathrm{d}E/\mathrm{d}x$ cut by trigger counters for $\bar{p}$'s of $P_{\mathrm{init}} = 1.67$ GeV/c. $1/\beta_{\mathrm{T3-T1}}$, $1/\beta_{\mathrm{T4-T3}}$, and $\mathrm{d}E/\mathrm{d}x_{\mathrm{T4}}$ are shown in (a), (b), and (c), respectively. The hatched histogram indicates events survived after applying BID0.

The incident kinetic energy at the top of instrument (E_{TOI}) was derived from $\beta_{\mathrm{T4-T3}}$. The accuracy of energy determination was 1% in the very low energy region around 0.2 GeV where energy resolution is important. Around 1 GeV, energy determination is obtained with 5% accuracy. Systematic error of the absolute energy is estimated to be $\pm$ 1% due to calibration of the time of flight measurements and energy losses in the beam line. The incident position and angle were obtained by extrapolating the beam track to the BESS detector considering the fringing field produced by the BESS solenoidal magnet. The accuracy of the incident position and angle around 1 GeV were 2.5 mm and 2 mrad (rms deviation), respectively.

In order to compare the beam data and BESS MC results, a MC data set was generated as follows. To estimate interaction and energy losses in T4 and AC, which were located just upstream of BESS, they were included in the simulation. Input kinematics of beam particles was obtained by beam data event by event; i.e., the incident position and angle were determined by beam track, while the incident energy was determined by $1/\beta_{\mathrm{T4-T3}}$. This allows comparisons between beam data and MC results under the same conditions. Data sets are referred to as BEAM and MC, respectively.

5.2 Additional beam identification for BESS

Although beam identification was performed by BID0 as mentioned above, contamination on $\mathrm{N_{inc}}$ due to interaction and/or scattering of incident particles after DC2 was not negligible. It is therefore important to ensure that incident particles arrive at the top of instrument by adding cuts to BID0, with information from the upper TOF hodoscope being used for this purpose. Such information must be carefully used so as not to reject interaction events occurring in BESS.

In addition to BID0, the following cuts were applied:

(1) number of hits in the upper TOF hodoscope is one or more;
(2) beam trajectory agrees with upper TOF hit position in both r-ϕ and y-z plane.

These cuts are referred to as BID1, which includes BID0.

Under this approach, an incident particle is guaranteed to pass through T4 and AC without large angle scattering or interaction. The percentage of BID1 rejected events which interacted in the BESS instrument is only 1% at most, whereas most interacted events in T4 or AC are rejected.

After applying BID1, the mass of the incident particle was calculated using the incident velocity determined from the TOF measurement between T4 and the upper TOF; a value should be consistent with that of $\bar{p}$'s. Since the BEAM and MC mass distributions showed very good agreement, it is concluded that BID1 completely removes the effect of T4 and AC such that $\mathrm{N_{inc}}$ is precisely determined.

5.3 Systematic errors in beam experiment

Precise estimation of systematic errors and making accurate corrections are critical to obtain absolute value of the efficiencies. Possible sources of beam related systematic errors are

(1) beam dump effect;
(2) accidental track identification;
(3) beam identification using the upper TOF;
(4) accuracy of the beam energy determination.

Each of these errors is respectively evaluated.

5.3.1 Beam dump effect

With a $\bar{p}$ beam, some TOF counters recorded hits with delayed timing, i.e., around 0.7% of $\mathrm{N_{inc}}$, being the result of reentrant secondary particles generated by annihilation at the beam dump. Some of these tracks were observed in the JET chamber. To correct this effect on non-interacting efficiency when applying CUT, during off-line analysis the delayed hits were not included in the number of hits in upper and lower TOF hodoscopes; thereby eliminating the beam dump effect such that its correction was negligible. The resultant systematic error ($\delta\varepsilon_{\rm beam\,dump}$) is accordingly estimated as

$$\delta\varepsilon_{\rm beam\,dump} \sim 0.002.$$

5.3.2 *Accidental track identification*

An additional track was present in some events that was not related to a triggered particle. Such accidental tracks affect non-interacting efficiency when selecting a single particle event. Since "slow gas" is used in the BESS chambers (JET/IDCs), the drift time is relatively long so that accidental tracks can easily appear in the tracking detectors. Since production probability of an accidental track is in general proportional to incident beam intensity, accidental tracks appeared at most 3% of $N_{\rm inc}$, being about 1% for a $\bar{p}$ beam and below 0.3% for a proton beam according to beam intensity.

When applying the single particle selection of CUT, an accidental track should be ignored. However, the only way to determine if a multi track event is an accidental or actual interaction is to check whether or not it has a vertex inside the instrument. An accidental track which exists close to the track of a triggered particle would therefore be misidentified as an interaction. As this inefficiency is about 15%, the correction ($d\varepsilon_{\rm accidental}$) to the efficiency is estimated as

$$0.001 < d\varepsilon_{\rm accidental} < 0.005,$$

with the systematic error ($\delta\varepsilon_{\rm accidental}$) due to this correction being estimated as

$$\delta\varepsilon_{\rm accidental} < 0.001.$$

This value is smaller for protons due to smaller incident beam intensity.

5.3.3 *Beam identification using upper TOF*

As described in Section 5.2, BID1 can effectively confirm that non-interacting particles are incident into the BESS instrument. However, since CUT will also reject a small fraction of interacted events in BESS, a correction is needed. Using the BESS MC, the amount of correction ($d\varepsilon_{\rm beam\,ID}$) is estimated as

$$-0.01 < d\varepsilon_{\rm beam\,ID} < -0.005,$$

where it is equally applied to both BEAM and MC.

Evaluation of systematic error is also needed in terms of correspondence between BEAM and MC, being estimated by varying the cut parameters of BID1. The rms deviation of the difference in efficiency between BEAM and MC was used to represent the systematic error, i.e.,

$$\delta\varepsilon_{\mathrm{beam\,ID}} \sim 0.005,$$

which is comparable to the statistical error of the efficiencies. With this approach there is no large systematic error incurred using information from the upper TOF.

5.3.4 Accuracy of beam energy determination

Since there is systematic uncertainty of about $\pm$ 1% in beam energy determination, measured efficiency is affected where it changes rapidly with energy. In fact, it is difficult to reliably estimate the effect of systematic errors on measured efficiency in such an energy region.

5.3.5 Total error in direct measurement of non-interacting efficiency

The correction ($d\varepsilon$) and total error ($\delta\varepsilon$) in $\varepsilon_{\mathrm{non-int}}$ were obtained using

$$d\varepsilon = d\varepsilon_{\mathrm{accidental}} + d\varepsilon_{\mathrm{beam\,ID}}$$

$$\delta\varepsilon^2 = \delta\varepsilon^2_{\mathrm{statistic}} + \delta\varepsilon^2_{\mathrm{beam\,dump}} + \delta\varepsilon^2_{\mathrm{accidental}} + \delta\varepsilon^2_{\mathrm{beam\,ID}},$$

where $\delta\varepsilon_{\mathrm{statistic}}$ denotes the statistical error.

6 Results

6.1 Direct measurement of non-interacting efficiencies

Figure 5 shows for each configuration the non-interacting efficiency for $\bar{p}$'s and protons derived from BEAM data and MC results. Note that the error bars include both statistical and systematic uncertainties while they are too small to see in the figure. Exceptionally close agreement between BEAM and MC occurs above ~0.2 GeV, although large discrepancies exist below this energy where non-interacting efficiency rapidly drops due to stopping of incident $\bar{p}$'s in the instrument. As mentioned in Section 5.3.4, such discrepancies may be due to the accuracy of the beam energy determination, with systematic uncertainty

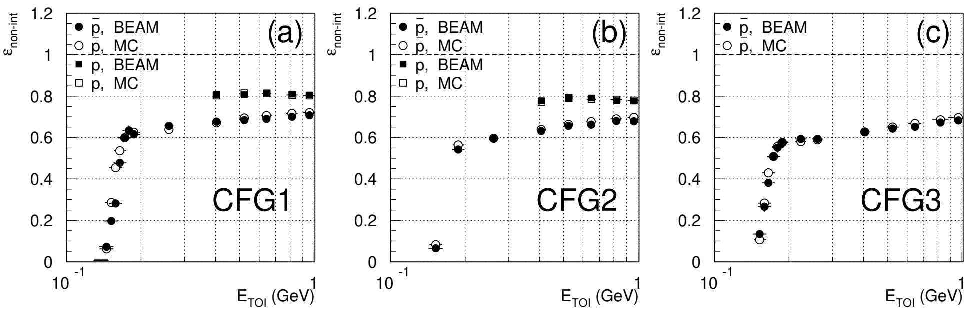

Fig. 5. Direct measurement of non-interacting efficiency for $\bar{p}$'s and protons in (a) CFG1 , (b) CFG2 , and (c) CFG3 .

of the measured efficiency being very large if the beam energy is assumed to be accurate.

6.2 Relative difference in non-interacting efficiency between beam and BESS MC data

The relative difference in non-interacting efficiency between BEAM and MC ($(\Delta\varepsilon/\varepsilon)_{\rm non-int} = (\varepsilon_{\rm MC} - \varepsilon_{\rm beam})/\varepsilon_{\rm beam}$) for $\bar{p}$'s and protons is shown in Fig. 6 from 0.16 to 1.0 GeV for $\bar{p}$'s (0.4 to 1.0 GeV for protons), where the measured data can be used as a reference of the non-interacting efficiency with well-estimated errors. Note that good agreement between BEAM and MC exists for

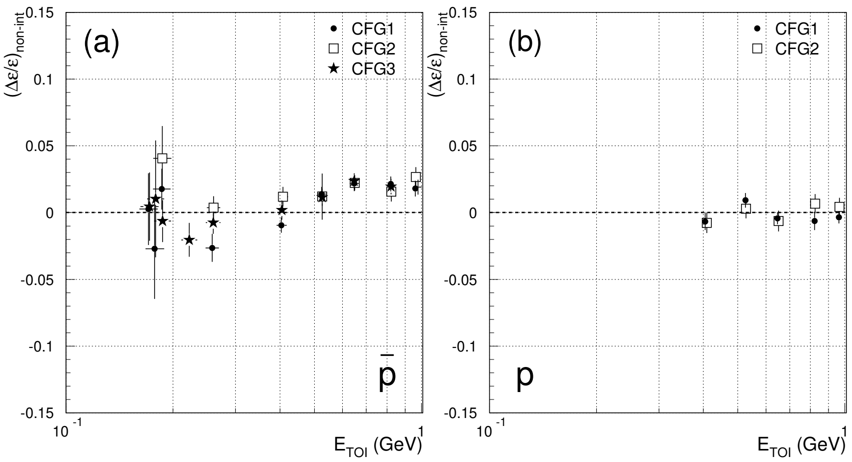

Fig. 6. Relative difference in non-interacting efficiency of MC from BEAM for (a) $\bar{p}$'s and (b) protons.

all configurations, where $(\Delta\varepsilon/\varepsilon)_{\mathrm{non-int}}$ is within $\pm$ 5% (2%) for $\bar{p}$'s (protons). Since each point of Fig. 6 corresponds to the systematic discrepancy of non-interacting efficiency derived from BESS MC data for a given energy and configuration, these results are considered to clearly indicate that above 0.16 GeV (for protons above 0.4 GeV) calculated efficiencies are correct within $\pm$ 5%, although for $\bar{p}$'s above 0.5 GeV small but significant discrepancies are present.

7 Discussion

While non-interacting efficiency has been directly measured, BESS MC results are nevertheless needed to estimate the non-interacting efficiency because (i) efficiencies over the whole BESS fiducial are required, (ii) the detection capability of $\bar{p}$'s ranges up to 4.2 GeV, and (iii) the configuration of BESS has changed year by year. Since non-interacting efficiency is the output of complex processes, a detailed systematic study of the BESS MC simulation is essential to evaluate its reliability. Systematic errors in the simulation should accordingly be evaluated using the results obtained in the previous section. Together with this, sources of discrepancies in non-interacting efficiency for $\bar{p}$'s above 0.5 GeV will be discussed.

7.1 Systematic study of BESS MC related to material amount

The amount of material included in the simulation was investigated first. Proton and helium (albedo proton) samples in flight data can be used to examine the amount of material in the lower (upper) half of the instrument. That is, if the stopping energy is defined as the energy where $\mathrm{d}E/\mathrm{d}x$ in lower (upper) TOF counter begins to decrease due to the incident particle being stopped inside the counter, then the stopping energy of these samples measured in the JET provides the total energy loss of the incident particle after it, a behavior that was well-reproduced by the simulation. Regarding BEAM data, on the other hand, the stopping energy for CFG1 and CFG3 is 0.154 and 0.160 GeV, respectively, being in good agreement with simulation results within $\pm$ 2 MeV and close to the accuracy of the incident energy determination. The BESS MC is therefore correct in terms of the amount of material.

7.2 Systematics of BESS MC related to interactions

Interaction processes, being the most important feature of the simulation, were investigated secondly. Antiproton events in MC can be classified into four categories, i.e.,

(1) no interaction (including delta-ray and multiple scattering effect);
(2) elastic scattering (diffraction scattering);
(3) inelastic scattering (incident $\bar{p}$ survives);
(4) annihilation.

Note that (2) – (4) are processed in a hadronic package. Generally, about 70 to 90% of the elastically scattered events pass through CUT, while it rejects most inelastically scattered and annihilated events; although in comparison, inelastically scattered events have a higher survival probability. It is important to realize that survival probability is dependent on the interaction point in the instrument and hadronic packages. Figure 7 shows the inelastic and elastic cross sections for $\bar{p}$ to aluminum used in the BESS MC, as well as those of the original GHEISHA code, FLUKA code, and experimental data [15]. Note that the inelastic cross section includes both inelastic scattering and annihilation processes. The solid curves are fit with these data points and used in the BESS MC.

To study hadronic interaction processes, it is beneficial to compare GHEISHA results with a different hadronic package. Accordingly, we used FLUKA [19] implemented in GEANT3.21 (GFLUKA). This version of FLUKA, however, is out of date because the FLUKA standalone code has undergone continuous development over the last decade.

Our investigation showed that

(1) The inelastic scattering probability is different between GHEISHA and GFLUKA, with that of GFLUKA being overestimated whereas that of GHEISHA is reasonable (see Section 7.2.1 for details);
(2) For annihilation cases, although GHEISHA exhibits some problems in secondary multiplicity and angular distribution such that GFLUKA is preferred, this discrepancy does not affect the non-interacting efficiency (see Section 7.2.2 for details);
(3) Losses due to elastic scattering are larger in GHEISHA than in GFLUKA because of the difference in angular distributions, with GHEISHA being preferred since non-interacting efficiency agrees better with BEAM using empirically determined cross sections.

Based on these findings, we conclude that GHEISHA is sufficiently reliable for our purpose.

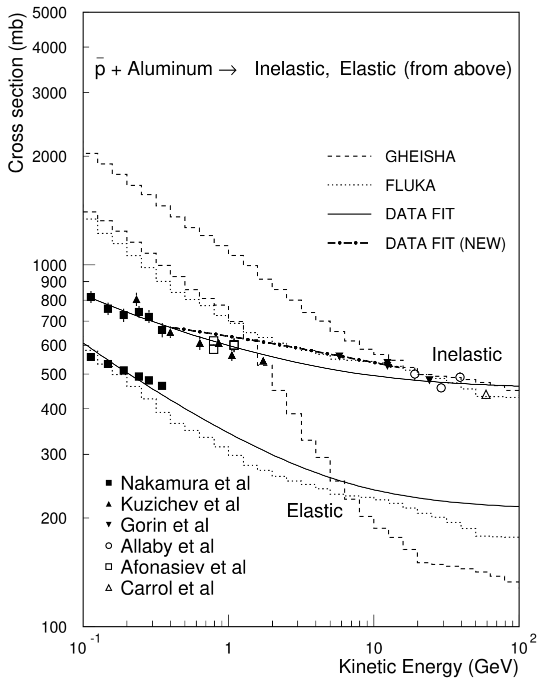

Fig. 7. Inelastic and elastic cross sections for $\bar{p}$ to aluminum. Histograms are from the GHEISHA and FLUKA codes and data points [15] from Nakamura et al. (filled squares); Kuzichev et al. (filled triangles); Gorin et al. (inverted triangles); Allaby et al. (open circles); Afonas'ev et al. (open squares); and Carroll et al. (open triangles). The solid curves are fit with these data points and used in the BESS MC. The dash-dot curve is a new fit that better reproduces the results of the beam experiment.

Finally, surmising that about 10% relative error is present in our empirical fit (solid curve of Fig. 7) to the $\bar{p}$-nuclei cross section data, it then seems reasonable to tune them in order to reproduce $\varepsilon_{\mathrm{non-int}}$ of BEAM for $\bar{p}$'s above 0.5 GeV. Moreover, among all measured $\bar{p}$-nuclei cross section data, that of Kuzichev et al. [15] are annihilation cross sections not total inelastic cross sections. Therefore, assuming about 10% probability of inelastic scattering in this energy range, which is consistent with the GHEISHA code, we refit the data below 15 GeV. With this approach to using these cross sections (see dash-dotted line of Fig. 7), $\varepsilon_{\mathrm{non-int}}$ was well reproduced up to 1 GeV.

Several kinds of implementation of hadronic packages are used to study the effect of differences in cross sections, generation of secondary particles, and their effects on efficiencies, i.e.,

GHEISHA(ORIG) : original GHEISHA;
GHEISHA(BESS) : GHEISHA with total inelastic cross section modified for BESS (solid line of Fig. 7);

GHEISHA(NEW) : GHEISHA with total inelastic cross section further modified for BESS (dash-dot line of Fig. 7 and Kuzichev adjusted);
GFLUKA(ORIG) : original GFLUKA, referred to as GFLUKA(ORIG);
GFLUKA1 : GFLUKA with same inelastic cross section as GHEISHA(BESS);
GFLUKA2 : GFLUKA with same inelastic cross section and same probability of inelastic scattering as GHEISHA(BESS);
GFLUKA3 : GFLUKA tuned by total inelastic cross section to reproduce non-interacting efficiency of BEAM data.

7.2.1 Cross sections

Data of both $\bar{p}$'s and protons were taken using a configuration in which a 30-mm-thick aluminum plate was placed just upstream of the BESS detector (see CFG$1_{+\mathrm{Al}}$ of Table 2).

A check of the $\bar{p}$-aluminum cross sections was performed by comparing the non-interacting efficiency assuming that the aluminum plate was included in the BESS instrument. When an interaction occurs in the aluminum, it is assuredly well detected in the BESS detector regardless whether the event is annihilation or inelastic scattering. Good agreement within $\pm$ 2% was obtained with GHEISHA (BESS) when the aluminum plate was placed in the same position, while $\varepsilon_{\mathrm{non-int}}$ decreased by $\approx$ 10%. However, a discrepancy of the same magnitude ($\Delta\varepsilon_{\mathrm{non-int}} \approx 0.015$) was found for $E_{\mathrm{TOI}} > 0.5$ GeV as shown in Fig. 6. On the other hand, when using GFLUKA3 as the hadronic package, $\Delta\varepsilon_{\mathrm{non-int}} \approx -0.015$ was obtained for $E_{\mathrm{TOI}} > 0.5$ GeV while GFLUKA3 well reproduced $\varepsilon_{\mathrm{non-int}}$ without the aluminum plate. These results can be explained by the overestimation of inelastic scattering probability in GFLUKA.

7.2.2 Multiplicity and angular distribution of secondary particles

When efficiencies are compared at each reduction step of CUT, if GHEISHA (BESS) was used as the hadronic package, then the difference in efficiencies between BEAM and MC becomes smaller as the cuts are added together. In contrast, however, with GFLUKA2 this difference did not change as the cuts were added together. Since both these hadronic codes have the same elastic and inelastic cross sections, this behavior is due to secondary multiplicity and angular distribution.

The discrepancy between BEAM and MC(GHEISHA(BESS)) should therefore be observed in the distribution of secondaries generated during instrument interactions. This was accordingly investigated by comparing the timing difference (Δt_{U}) between upper TOF counters using the events of $\mathrm{N_U} > 1$ for $\bar{p}$'s as shown in Fig. 8, where $\mathrm{N_U}$ indicates the number of hit counters in the upper TOF. The vertical axis is normalized to total incident $\bar{p}$'s, and Δt_{U}

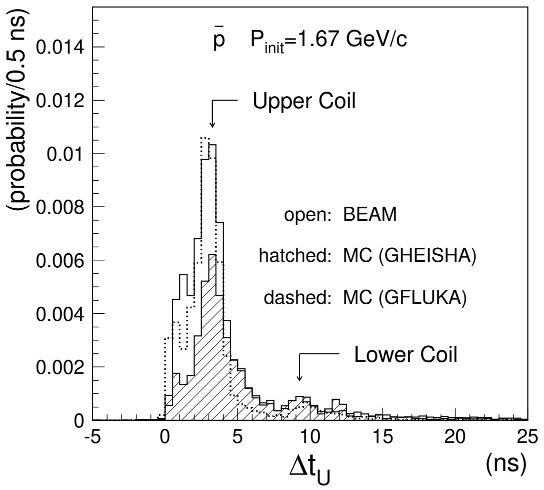

Fig. 8. Δt_{U} distribution for multiple hits in upper TOF excluding adjacent hits which smear the effect of instrument interactions with the large peak at $\Delta t_{\mathrm{U}} = 0$. Open, hatched, and dashed histograms correspond to BEAM, MC(GHEISHA(BESS)), and MC(GFLUKA2).

corresponds to the sum of the time of flight of an incident particle from the upper TOF counter to the interaction point and that of a secondary particle from the interaction point to another upper TOF counter. The peaks around 3 and 10 ns correspond to events in which interaction occurred at the upper and lower coil, respectively. The discrepancy seen in the peak around 3 ns clearly indicates that the rate of secondaries generated toward the upper TOF hodoscope is higher in BEAM than in MC(GHEISHA(BESS)) for $\bar{p}$'s. On the other hand, a comparison of Δt_{U} shows good agreement for protons (not shown). The discrepancy in the Δt_{U} distribution accordingly indicates that the GHEISHA code has some problems in reproducing secondary multiplicity and angular distribution in cases of annihilation events. The dotted histogram in Fig. 8 corresponds to results obtained using GFLUKA2 vice GHEISHA (BESS), where in terms of secondary distribution, GFLUKA is preferred to GHEISHA.

In the case of annihilation, when comparing the survival probability of CUT between GHEISHA(BESS) and GFLUKA2, the difference is less than $\pm$ 0.3%, and GHEISHA(BESS) gives higher probability on the average. Thus, even though GHEISHA exhibit some problems in secondary multiplicity and angular distribution for annihilation events, the effect on non-interacting efficiency is quite small. This is because of excellent capability of detecting interactions with much independent information and uniform performance of the BESS detector.

7.3 Systematics of BESS MC related to detector descriptions

The detector description in the BESS MC was also investigated. As previously mentioned, estimating the effect on $\varepsilon_{\rm non-int}$ due to discrepancies in the detector description in MC is complicated because distinguishing those in the detector description from those in hadronic processes is difficult. However, no discrepancy need be explained by detector response because $\varepsilon_{\rm non-int}$ was successfully reproduced by the BESS MC for all configurations for $\bar{p}$'s and protons, with BESS MC estimating only a 1% loss for non-interacted events when applying CUT. Losses are instead caused for example by adjacent TOF hits, tail of the dE/dx distributions, or other reasons. Furthermore, since CUT for $\varepsilon_{\rm non-int}$ is a geometrical and loose cut which removes only tails of the distribution, it should be robust against detector response and calibration, while this is not the case for determining efficiency which includes a track quality cut such as reduced χ^2 and number of fitted points selection. Thus, possible discrepancies in detector description are not considered to affect the non-interacting efficiency.

7.4 Reproduction of non-interacting efficiency for various configurations

Since it is impossible to completely reproduce interaction processes and detector response, reproducibility of efficiencies for various configurations is important. To study this, the maximum deviation of $\Delta\varepsilon_{\rm non-int}$ between all configurations ($\delta\varepsilon_{\rm CFG}$) were calculated for all energies, i.e.,

$$\delta\varepsilon_{\rm CFG} \sim 0.005.$$

Since CFG1–3 were selected to represent the incidence of cosmic-ray particles in terms of the amount of material and tracking region, the fact that $\delta\varepsilon_{\rm CFG}$ was kept sufficiently low demonstrates the validity of the non-interacting efficiencies derived from BESS MC over the whole fiducial region.

7.5 Comparison of identification efficiency with BESS MC data

Identification efficiency was investigated lastly. While it can be estimated using unbiased proton samples in the flight data, the assumption that $\varepsilon_{\rm ID}(\bar{p}) = \varepsilon_{\rm ID}(p)$ must be confirmed using BEAM data. Figure 9 shows the $\bar{p}/p$ ratio of the identification efficiency ($r_{\rm ID} \equiv \varepsilon_{\rm ID}(\bar{p})/\varepsilon_{\rm ID}(p)$), where the open histogram indicates MC data in which an isotropic beam was incident to the instrument such that a value of unity was present over the whole energy range. Note that $r_{\rm ID}$

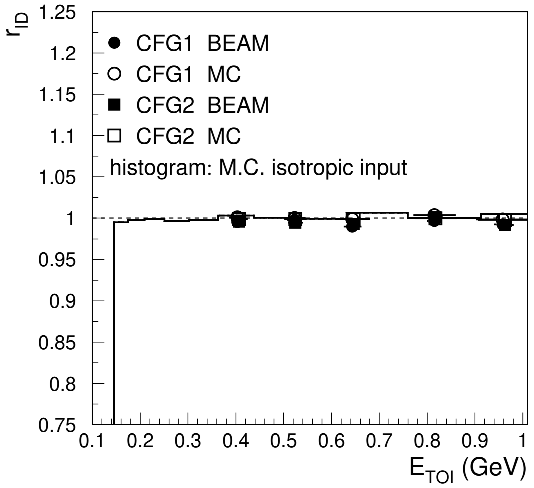

Fig. 9. The $\bar{p}/p$ ratio of the identification efficiency. The open histogram indicates MC data in which an isotropic beam was incident to the instrument.

of BEAM shows good agreement with the histogram and MC, which confirms that $\varepsilon_{\rm ID}$'s were the same for protons and $\bar{p}$'s; hence "visible" interactions are completely removed by CUT and only non-interacting efficiency contributes to the systematic error due to interaction losses in detection efficiency.

7.6 Systematic error in detection efficiency

Since the BESS MC was validated and $\varepsilon_{\rm ID}(\bar{p}) = \varepsilon_{\rm ID}(p)$ was confirmed, the systematic error in detection efficiency over the whole BESS fiducial can be evaluated by the relative differences in non-interacting efficiency between BEAM and MC. Based on the efficiency calculation in flux measurements (efficiencies are averaged over the whole acceptance region), all data of CFG1–3 were combined and $\delta\varepsilon_{\rm CFG}$ were added into the errors for each data point. This is shown in Fig. 10 together with the systematic error used in the previous analysis, being estimated as 15, 12, and 10% in the energy range of $<$ 0.3, 0.3–0.5, and 0.5–1.0 GeV, respectively. As shown, the accelerator beam calibration confirmed that the BESS MC gave reasonably correct detection efficiencies, and reduced the systematic error in detection efficiency for $\bar{p}$'s to within 5 and 4% from 0.16 to 0.3 and 0.3 to 1.0 GeV, respectively; and for protons to within 2% from 0.4 to 1.0 GeV (represented by closed circles obtained with GHEISHA(BESS)). In addition, the use of modified cross sections reproduces detection efficiency exactly and the systematic error in detection efficiency can be reduced to $\pm$ 2% from 0.3 to 1 GeV for $\bar{p}$'s (represented by open circles obtained with GHEISHA(NEW)).

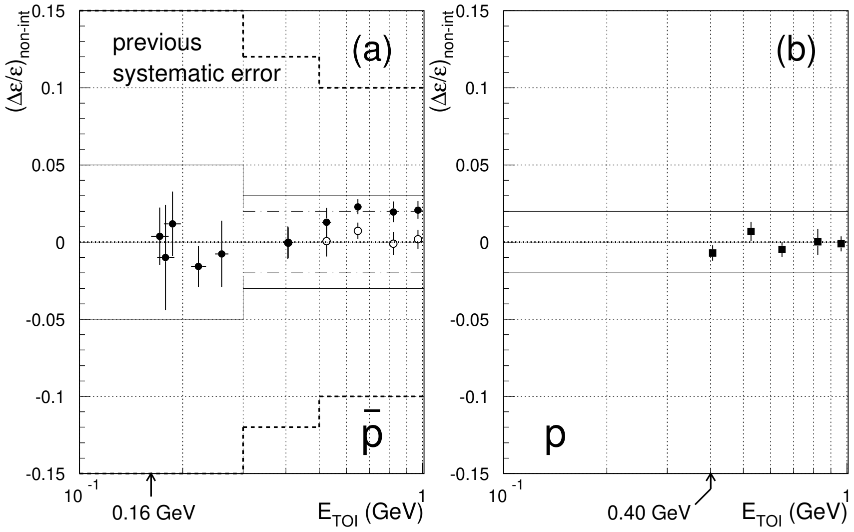

Fig. 10. Test of the detection efficiency derived from BESS M.C. for (a) $\bar{p}$'s and (b) protons. Closed circles represent relative differences between BEAM and MC(GHEISHA(BESS)) when combining all configurations, while open circles are obtained with GHEISHA(NEW). The dashed line in (a) is the previous systematic error attributed to detection efficiency.

Discrepancies in non-interacting efficiency above 0.5 GeV have now been discussed in detail and the BESS MC itself is well understood, thus allowing the systematic error in detection efficiency above 1 GeV to be estimated. That is, based on the relative difference in non-interacting efficiency among several hadronic packages (GHEISHA(BESS), GHEISHA(NEW), GFLUKA(ORIG), GFLUKA2, and GFLUKA3), the systematic error in detection efficiency above 1 GeV is estimated to be within $\pm$ 5%.

8 Summary and Conclusions

Through the accelerator beam experiment, the absolute calibration of the detection efficiency for $\bar{p}$'s and protons were performed below 1 GeV, and the BESS Monte Carlo simulation was verified in detail. The calibration remarkably reduced the relative systematic error in detection efficiency derived from the simulation, especially for $\bar{p}$'s. It can be applied to systematic errors in cosmic-ray $\bar{p}$ measurements (i.e., $\bar{p}$ flux[8–10]), as well as forth coming data from 1999/2000 flights and future BESS experiments including high statistics long-duration flights[20] providing the instrumental features of BESS are maintained. By increasing the reliability of the cosmic-ray $\bar{p}$ spectrum, these results will enable us to carry out the most sensitive-ever investigation on the origin of cosmic-ray $\bar{p}$'s.

Acknowledgements

We appreciate support during accelerator beam experiments by Mr. M. Taino, Dr. M. Ieiri (KEK), Dr. A. Ichikawa (Kyoto Univ.), Mr. H. Takahashi (Kyoto Univ.), and other members of E373 group. We also thank Mr. S. Tsuno (Tsukuba Univ.) and Dr. H. Iwasaki (KEK) for allowing use of their drift chambers (DC1, DC2). This work was supported by a Grant-in-Aid for Scientific Research from the Japanese Ministry of Education, Science and Culture. Analysis was performed using the computing facilities at ICEPP, the University of Tokyo. Some of the authors were supported by Japan Society for the Promotion of Science.

References

[1] S. Orito, in Proceedings of the ASTROMAG Workshop (KEK Report 87-19, 1987), p.111.

[2] A. Yamamoto et al., Adv. Space Res. **14**, (1994)(2) 75

[3] Y. Ajima et al., Nucl. Instrum. Methods A **443**, (2000) 71

[4] A. Yamamoto et al., IEEE Trans. Magn. **24**, (1988) 1421.

[5] Y. Asaoka, K. Abe, K. Yoshimura et al., Nucl. Instrum. Methods A **416**, (1998) 236

[6] Y. Shikaze, T. Mitsui et al., Nucl. Instrum. Methods A **455**, (2000) 596

[7] K. Yoshimura et al., Phys. Rev. Lett. **75**, (1995) 3792; A. Moiseev et al., Astrophys. J. **474**, (1997) 479.

[8] H. Matsunaga et al., Phys. Rev. Lett. **81**, (1998) 4052.

[9] S. Orito et al., Phys. Rev. Lett. **84**, (2000) 1078.

[10] T. Maeno et al., astro-ph/0010381, to be published in Astropart. Phys.

[11] S. W. Hawking, Commun. Math. Phys. **43**, (1975) 199.

[12] H. Matsunaga, Ph.D. thesis, The University of Tokyo. 1997.

[13] R. Brun et al.., GEANT3.21, CERN Program Library Long Write up W5013.

[14] H. Fesefeldt, PITHA 85/02, Aachen, 1985.

[15] K. Nakamura et al., Phys. Rev. Lett. **52**, (1984) 731. V. F. Kuzichev et al., Nucl. Phys. A **576**, (1994) 581. Yu. P. Gorin et al., Yad. Fiz. **18**, (1973) 336. J. C. Allaby et al., Yad. Fiz. **12**, (1970) 538. V. N. Afonas'ev et al., Yad. Fiz. **40**, (1984) 34. V. N. Afonas'ev et al., Yad. Fiz. **47**, (1988) 1656. A. S. Carroll et al., Phys. Lett. B **80**, (1979) 319.

[16] R. K. Tripathi et al., Nucl. Instrum. Methods B **155**, (1999) 349.

[17] A. Yamamoto et al., Nucl. Instrum. Methods A **203**, (1982) 35.

[18] K. Nakazawa, Nucl. Phys. A **585**, (1995) 75c; A. Ichikawa, et al., Nucl. Instrum. Methods A **220**, (1998) 417.

[19] A Fasso', et al., Proc. IV Int. Conf. on Calorimetry in High Energy Physics, La Biodola, Italy, 1993, p. 493.

[20] A. Yamamoto et al., Proc. of COSPAR-2000, to be published in Adv. Space Res.